Crystallographic and Fractographic Studies of Hydrogen-Induced Cracking in Purified Iron and Iron-Silicon Alloys

F. NAKASATO AND I. M. BERNSTEIN

Crystallographic and fractographic studies have been carried out on hydrogen charged purified iron and on iron-silicon alloys with silicon contents up to 3 pct. The specimens could be cracked by cathodically charging with hydrogen even without the application of an external stress. An experimental technique was developed which enabled the exposure of the fracture surface formed purely by hydrogen charging, and to contrast this with an adjacent mechanically induced fracture surface. In the case of purified iron, hydrogen induced cracks are found to occur on potential slip planes whereas in the case of iron-3 pct silicon, the crack follows the observed cleavage plane. Intermediate silicon content alloys showed transitional behavior. In agreement with the variation of crack plane in the alloys, the fracture surface appearances was also drastically different, reflecting the change in intrinsic toughness with alloy content. The observed transition from slip plane cracking to cleavage plane cracking was found to occur near a silicon content of 0.7 pct. The observed behavior is discussed in terms of how the intrinsic toughness of the iron-based lattice affects how hydrogen-induced cracks are formed.

ALTHOUGH hydrogen-induced cracking in ferrous alloys has been studied extensively from both the fundamental and practical points of view, its fractographic and crystallographic nature is still a subject of dispute. Recently, fractographic studies have revealed that plastic deformation can play an important role in the process of hydrogen induced crack growth[1] and that it is not sufficient to interpret hydrogen embrittlement as a simple extension of cleavage fracture.[2] The crystallographic nature of transgranular hydrogen induced cracks, from the results Tetelman and Robertson,[3,4] and Gell and Robertson[5] who examined iron-3 pct silicon single crystals, is generally accepted as {100} cracks, the usual cleavage planes of α-iron.[6,7] Their results were obtained by observing the relative positions of etch pit arrays of dislocations and one surface analysis of crack traces.

More recently, conflicting data have questioned the generality of this result. Bernstein[8,9] from a one-surface trace analysis in purified polycrystalline iron, suggested instead that hydrogen induced transgranular cracks, in the absence of an external stress, occur on the potential slip planes, {110} or {112}.[8,9] Terasaki and Nakasato[2] also demonstrated the existence of a (101) crack in hydrogen charged and externally stressed iron single crystal. In conflict with these results, Kitajima[10] has claimed that the fracture surfaces are macroscopically along {100} planes in both iron single crystals and iron-3 pct silicon single crystals under conditions of hydrogen charging and external stressing. For hydrogen charging only in iron-3 pct silicon polycrystals, Kikuta *et al*[11] deduced, from the shape of facet pits directly on the fracture surface, that there was a transition of crack plane from {100} to {110} planes with increasing charging time of hydrogen.

In light of these conflicting results obtained for similar materials, it was deemed appropriate to re-examine the crystallographic and fractographic nature of hydrogen induced cracking. A comparative study was also made of the fracture surfaces formed solely by hydrogen charging with those only of mechanical origin in both purified iron and a series of iron-silicon alloys, with silicon content up to 3 pct, in order to determine if the details of environmentally and mechanically induced fracture are similar.

EXPERIMENTAL PROCEDURE

The concentrations of interstitial solutes and silicon in the alloys of this study are given in Table I.* A bi-

*The base iron was vacuum remelted, low interstitial Ferrovac-E iron.

crystal sheet of purified iron produced by the usual strain-anneal method was used for some of the crystallographic aspects of the study. Specimens $1.3 \times 2.5 \times 22$ mm in size were cut from sheets cold-rolled to a final thickness 1.3 mm. The heat treatments applied in the present investigation are schematically illustrated in Fig. 1, superimposed on the relevant portion of the iron-silicon phase diagram. Most specimens were heat-treated in evacuated quartz capsules at 850°C for 60 min followed by furnace cooling. The grain size obtained by the above heat treatment was about 200 μm. For several specimens of iron-3 pct silicon, a higher annealing temperature of 1300°C was also adopted to obtain larger grain sizes. After being held at 1300°C for 20 min, the specimens were furnace cooled to 850°C and held there for 60 min to insure a solute distribution similar to the other samples, followed by furnace cooling to room temperature. This heat treatment gave an average grain diameter of 1.5 mm. Furnace cooling was chosen, since previous studies showed

F. NAKASATO, formerly at Carnegie-Mellon University is now at Sumitomo Metal Industries Ltd., Central Research Laboratories, Amagasaki, Japan. I. M. BERNSTEIN is Professor, Department of Metallurgy and Materials Science, Carnegie-Mellon University, Pittsburgh, PA 15213.

Manuscript submitted February 27, 1978.

ISSN 0360-2133/78/0911-1317$00.75/0

Table I. Chemical Composition, Wt Pct

Material	C	N	O	Si
Bicrystalline Iron	0.005	0.001	0.002	0.03
Ferrovac-E	0.006	0.001	0.003	0.02
Fe-0.7 Pct Si	0.005	0.005	0.002	0.70
Fe-1.4 Pct Si	0.004	0.006	0.008	1.43
Fe-3 Pct Si	0.005	0.005	0.010	2.96

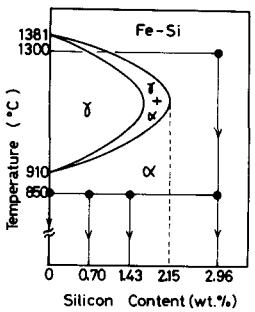

Fig. 1—Schematic diagram of heat treatments employed.

that the slower cooling rate promoted the preferred transgranular crackings during subsequent cathodic charging of hydrogen.[8,12,13] Cathodic charging was performed at room temperature in a 1 N sulfuric acid solution to which a recombination poison of 10 mg As_2O_5/l, plus 3 ml CS_2/l was added. The applied current density was 30 mA/cm^2, and the charging time was 12 h to ensure that a uniform distribution of hydrogen was present through the cross section of all specimens. No external stress was applied during hydrogen charging so that any stress assistance to cracking arose from residual stresses from molecular gas recombination at internal hydrogen sinks.[8] Any differences in behavior by using an externally applied stress will be subsequently considered. After hydrogen charging, the specimens were sectioned and any internal cracks were observed optically. For the bicrystal and the iron-3 pct silicon annealed at 1300°C, the crystallographic planes of hydrogen induced crackings were determined using the standard two-surface trace analysis. The crystallographic orientation of the specimens was determined by X-ray back-reflection Laue analysis.

Scanning electron microscopy was employed to characterize the fracture morphology. An experimental technique was established which enabled the exposure of the hydrogen induced crack surfaces formed in the absence of an external stress. Figure 2 is a schematic representation of the technique employed. A mechanical notch was very carefully introduced using a low speed diamond saw. The length of the mechanical notch was adjusted so that its tip was located close to a hydrogen induced crack revealed on the polished surface. After the introduction of the mechanical notch, the specimen was broken open by impact in liquid nitrogen, thereby linking the mechanical fracture surface to a hydrogen induced crack. When this technique was properly employed, a hydrogen induced crack surface could be observed on the broken surface of the specimen, together with a mechanically induced fracture surface. Thus, fractographic features of both types of crack surfaces could be studied.

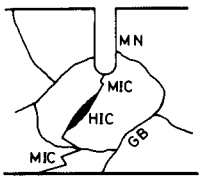

MN: Mechanical Notch
MIC : Mechanically Induced Crack
HIC : Hydrogen-Induced Crack
GB : Grain Boundary
Fig. 2—Experimental technique used for the exposure of hydrogen induced crack surfaces.

Tensile tests on the silicon-containing alloys were performed at room temperature at an initial strain rate of 8.5×10^{-4} s^{-1}.

EXPERIMENTAL RESULTS

A. Two-Surface Trace Analysis of Hydrogen-Induced Transgranular Cracks

Since no external stress was applied in the course of hydrogen charging, any anisotropy in stress should be minimized and it was expected and found that cracks which formed had more than one variant of any specific plane.

Examples of the hydrogen induced trans- and intergranular cracks in bicrystalline iron are illustrated in Fig. 3; the intergranular cracks are shown in the upper part of Fig. 3(*a*) but are not of interest to this study. Four transgranular cracks which form two sets of two mutually parallel cracks are also observed, designated on the Figure as cracks A, B, C, D. Cracks A and B are parallel to each other on the plane of observation, (h, k, l), shown to be near (110). Cracks C and D form another set of two parallel cracks. Figure 3(*b*) illustrates the two-surface trace analysis of crack A, where traces of crack A were observed on two orthogonal surfaces, designated by (h, k, l) and $(\bar{p}, \bar{q}, \bar{r})$, with the latter being near $(1, \bar{1}, \bar{1})$. The common direction shared by these two planes is near $[1, \bar{1}, 2]$, designated as [u, v, w]. Measurement of angles between the crack traces and the direction [u, v, w] on the two planes, (h, k, l) and $(\bar{p}, \bar{q}, \bar{r})$, establishes the indices of the crack plane. In this, crack A is found to be parallel to $(\bar{1}, 1, 0)$. A higher magnification picture of crack A is shown in Fig. 4, which shows that although considerable yawning has taken place, the fine crack near point A permits an accurate determination of the crack plane to be made. The arrow points to a step formed on the crack surface, which suggests that shear deformation leading to crack branching occurred during the expansion of the main crack. Crack B was also found to be parallel to $(\bar{1}, 1, 0)$ as expected. Similarly, cracks C and D were shown to be parallel to $(0, \bar{1}, 1)$, another variant of {110}. Traces of cracks C and D on (h, k, l) make an angle of approximately 90 deg with [u, v, w]; this observation completely excludes the possibility that cracks C and D can be variants of the usual {100} cleavage plane. A simple geometrical calculation shows that if crack C and D are assumed to be parallel to one of the {100} planes, the traces of these cracks

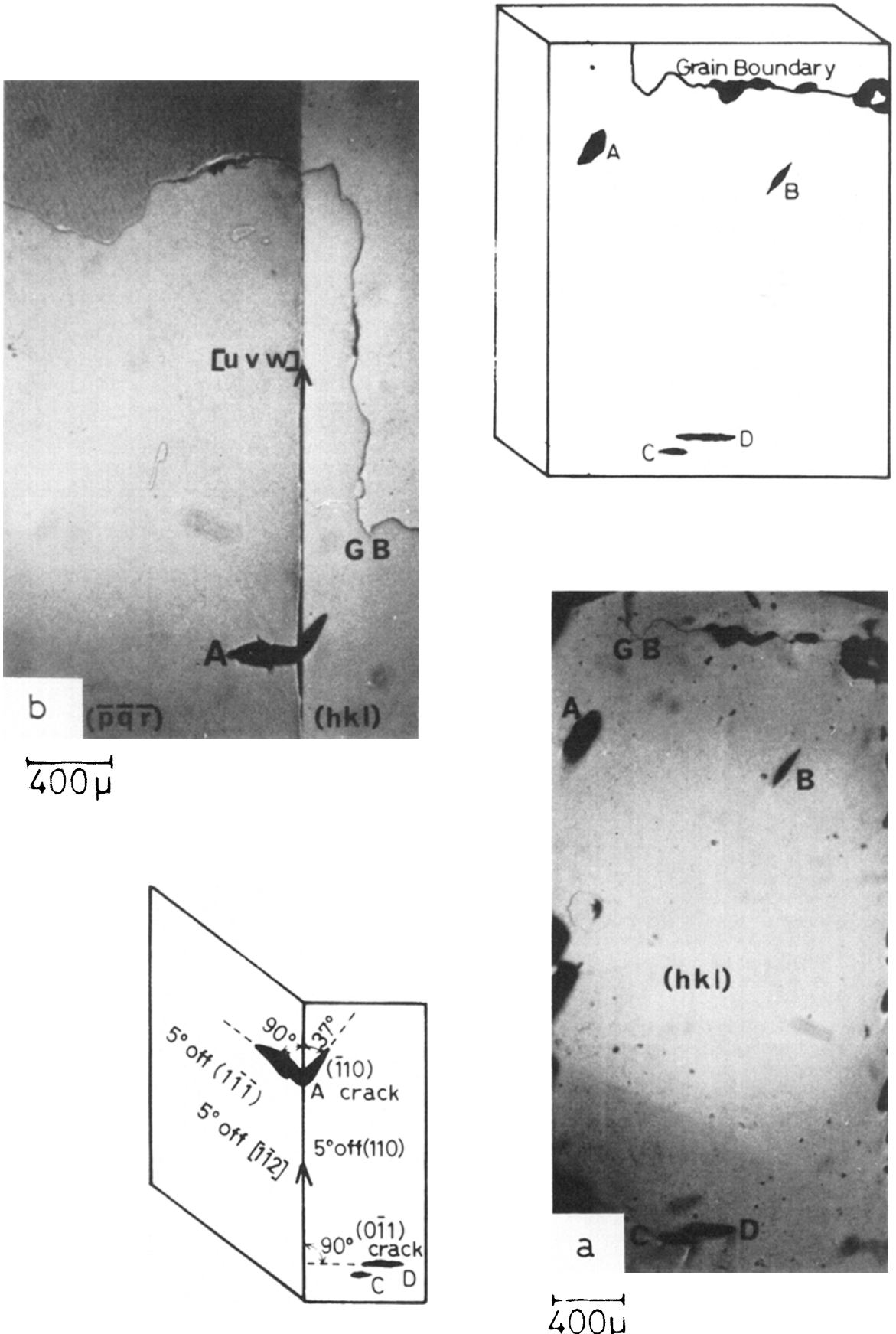

Fig. 3—Hydrogen induced trans- and intergranular cracks in a purified iron. (*a*) Notice the four transgranular cracks, A to D, which form two sets of two parallel cracks, (*b*) Example of a two-surface trace analysis, identifying (110) as the plane of crack A.

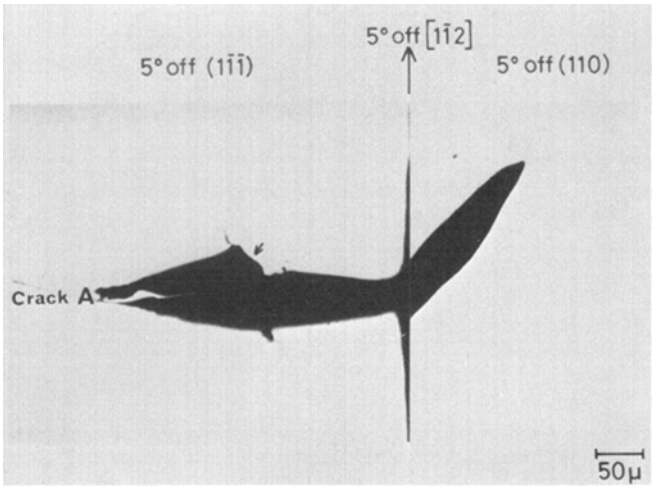

Fig. 4—Enlarged optical micrograph of crack A shown in Fig. 3.

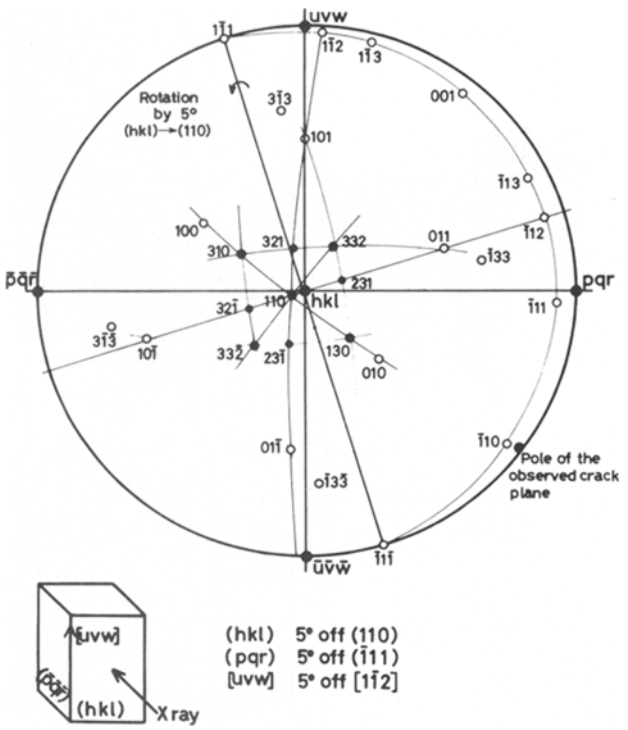

Fig. 5—Stereographic presentation of the observed plane of crack A. Note that the pole of the observed crack plane falls very close to ($\bar{1}$10).

on (h, k, l) should make angles of about 35 or 55 deg with [u, v, w], as opposed to the observed value of 90 deg. Figure 5 is a summary stereographic representation of the crack planes. Only a 2 deg variation between the pole of the crack plane and ($\bar{1}$, 1, 0) is found, well within experimental error. Additional confirmation of slip plane cracking is shown in Fig. 6, which is the third set of observed cracks, designated as cracks E and F. These cracks are not large enough for a two-surface trace analysis to be applied. One-surface trace analysis, however, strongly suggests that they are parallel to ($\bar{1}$, 1, 2), since their traces on (h, k, l) make an angle of 18 deg with [u, v, w], in good agreement with the value of 17 deg calculated under the assumption that crack E and F are parallel to ($\bar{1}$, 1, 2).

Figure 7 shows, in contrast, transgranular cracks observed in the hydrogen-charged iron-3 pct silicon annealed at 1300°C. The general shape of cracks observed in iron-3 pct silicon are substantially sharper than that in purified iron where cracks are expanded or "yawned", (Figs. 3 and 4). Four types of crack traces are shown in Fig. 7. Three of them are linear and two of these were found by two surface analysis to correspond to the two variants of {100} cracks. The third is believed to be the remaining third variant of a {100} crack as suggested by the results of one-surface trace analysis. The fourth crack appears to be noncrystallographic in nature. Such behavior was previously observed by Gell *et al*,[14] but only at −110°C and in iron-3 pct silicon single crystals. The complete stereographic analysis of crystallographic cracks in iron-3 pct silicon is shown in Fig. 8. The poles of observed crack planes fall close to {100} poles, but deviate far from {110} poles, confirming that the crystallographic cracks introduced in iron-3 pct silicon by cathodic charging of hydrogen at room temperature are parallel to one of the three {100} variants, but not to {110} or {112} as found in purified iron under the same experimental conditions. Possible reasons for such differences will be discussed.

B. Fractographic Study of Hydrogen-Induced Crack Surfaces

In the previous section, it was shown that with the addition of 3 pct silicon to purified iron the crystallographic planes of hydrogen-induced cracks changed from one of the operating slip planes, {110}, or possibly {112}, to one of the operating cleavage planes, {100}. In this section, a scanning electron microscopy study of hydrogen induced crack surfaces provides insight on the reasons for such differences.

Figure 9 shows a low magnification scanning electron micrograph of the fracture face of hydrogen charged bicrystalline iron. In the central portion of the micrograph, a hydrogen induced crack (HIC) surface is seen surrounded by a mechanically induced crack (MIC) surface. The edge of the polished surface is also shown. The temperature at which mechanical fracture took place was substantially above liquid nitrogen temperature, and therefore, the MIC surface indicates a ductile rather than a cleavage mode. In any event, the HIC surface is seen to be considerably different from the MIC surface. Blowups of hydrogen regions A and B in Fig. 9 are shown in Figs. 10 and 11, respectively. In Fig. 10, the hydrogen crack is characterized by planar segments and markings perpendicular to the advancing crack front. The striations on the crack face are taken as evidence that the cracking is discontinuous in nature. In addition, the crack face is seen to be not flat, but instead appears to be composed of planer segments, most likely other variants of the slip plane on which the major crack lies. Figure 11 is another typical crack surface appearance observed in hydrogen region, which looks somewhat different from Fig. 10. In Fig. 11, the crack surface appear composed of two distinct regions, E and T, which alternately run parallel to each other. Region E seems to be the part where the crack propagated relatively easily, leaving the markings per-

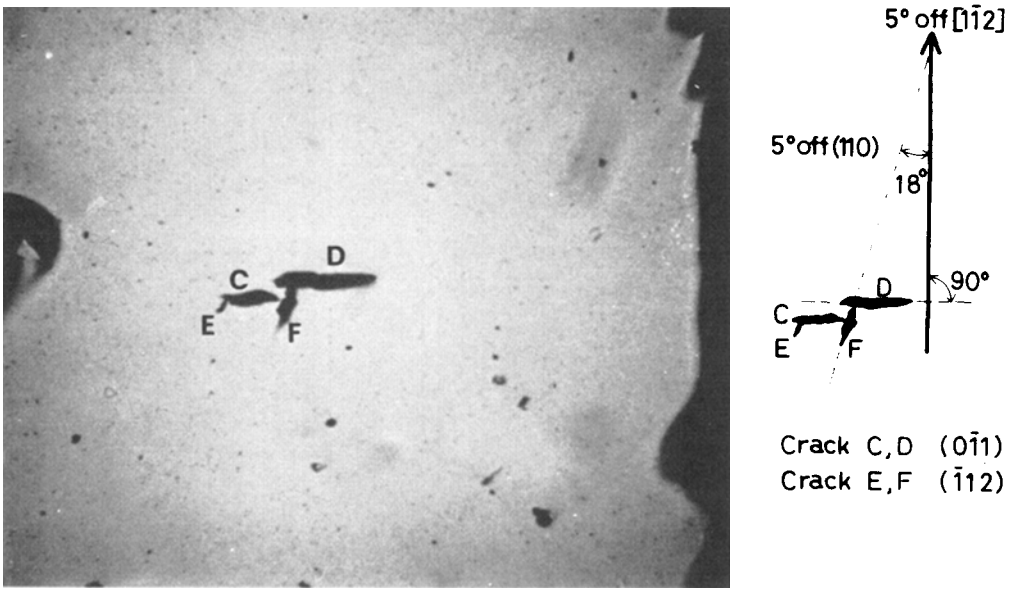

Fig. 6—Polished surface details near crack C and D in Fig. 3, exhibiting another set of two small parallel cracks, E and F. One-surface trace analysis suggests that these cracks are parallel to (1̄12).

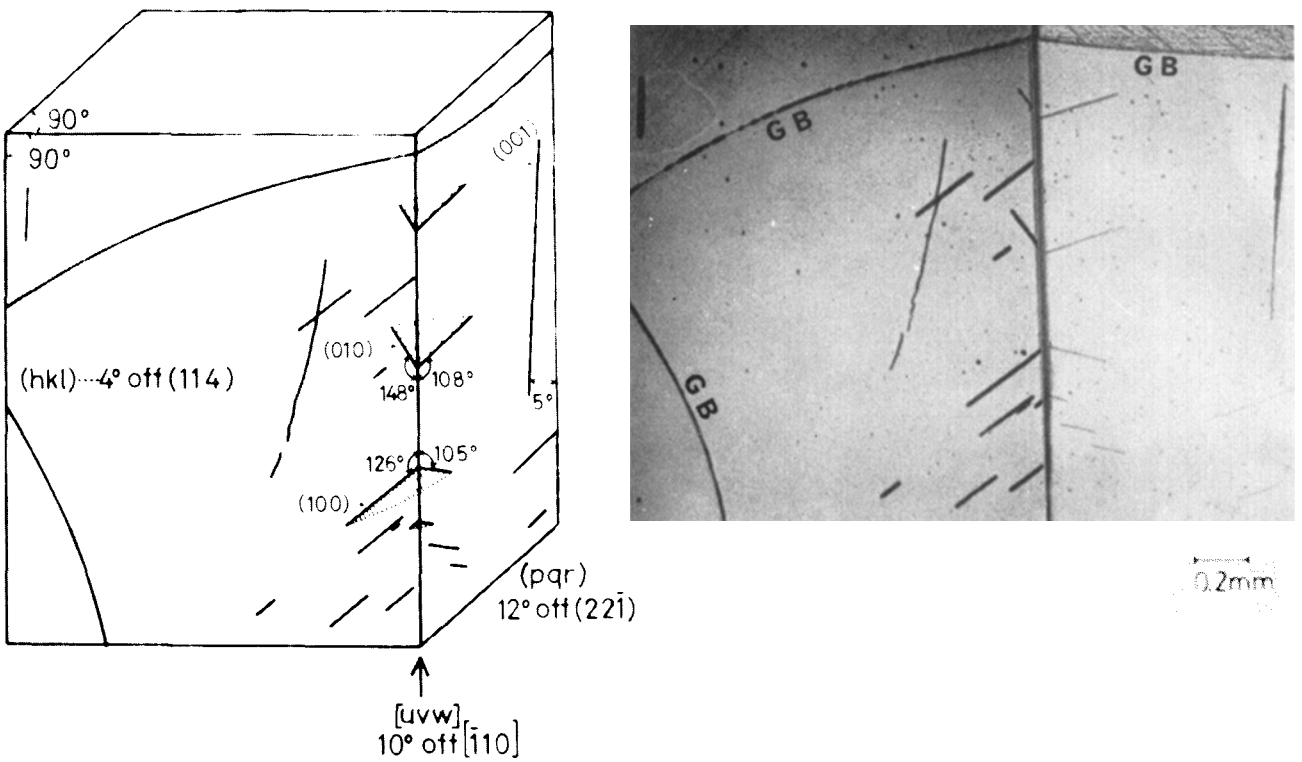

Fig. 7—Two-surface trace analysis of the transgranular cracks in hydrogen charged iron-3 pct silicon. Sharp crystallographic cracks lie on the three variants of {100} plane. Compare with Fig. 3. A noncrystallographic crack is also observed in the center of the picture.

pendicular to the direction of crack growth. On the other hand, region T is the tear ridge which links two adjacent regions of E.

Figure 12 compares a similar HIC surface but now with a low temperature cleavage crack surface in Ferrovac-E iron. Note the deformation twins introduced during the low temperature fracture. A blowup of the hydrogen region is found in Fig. 13. Note again the typical features of HIC, planar segments and markings perpendicular to the direction of crack propagation. The similarity between Figs. 10, 11 and 13 indicates that the HIC surface in purified iron is unique and can be distinguished from any type of fracture surface even in the presence of grain boundaries. Similar fractographic features have been reported for hydrogen charged and externally stressed iron single crystals,[2,15,16] suggesting similar behavior whether the stress necessary for crack extension is external or internal in origin.

Figure 14 shows a HIC surface formed in iron-3 pct silicon, together with an adjacent low temperature

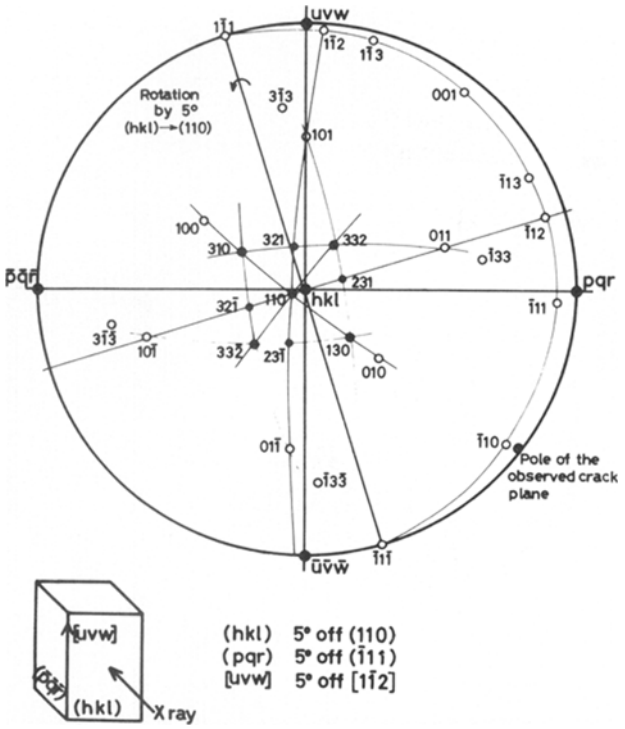

Fig. 8—Stereographic analysis of hydrogen induced transgranular cracks in iron-3 pct silicon. Note that the poles of the observed crack planes are close to {100} poles.

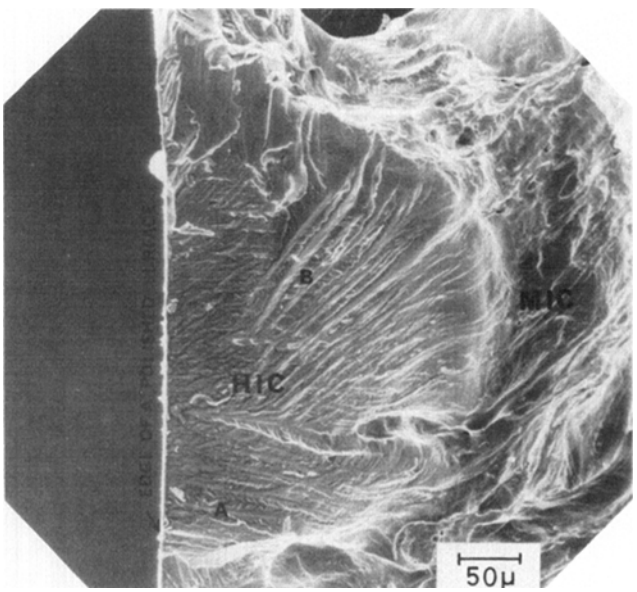

Fig. 9—Low magnification SEM photograph of the fracture face of hydrogen charged bicrystalline iron. HIC: Hydrogen induced crack, MIC: Mechanically induced crack.

cleavage crack surface mechanically induced at liquid nitrogen temperature. A deformation twin is observed to intersect both the HIC and MIC surface, forming a small step on the latter. Evidence for discontinuous cracking is not apparent on the HIC surface and the crack face is flat. Instead both regions show cleavage or river patterns. These observations demonstrate the similarity between the HIC surface and the low temperature cleavage crack surface in iron-3 pct silicon and contrast it sharply from the behavior in purified iron. Since HIC do not propagate catastrophically

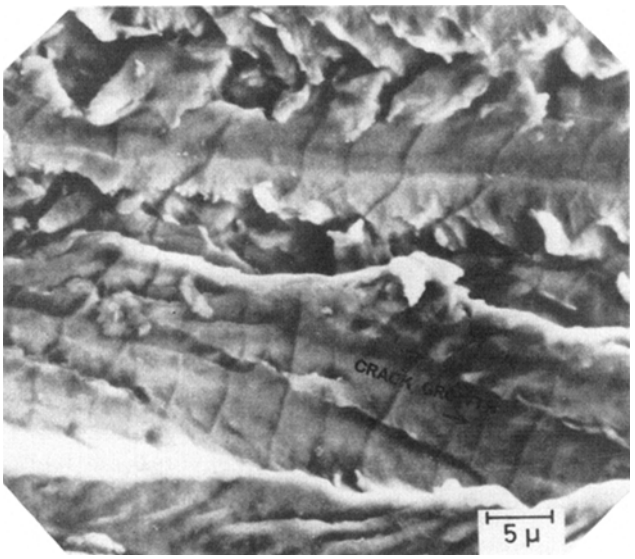

Fig. 10—Blowup of hydrogen region A in Fig. 9. Note the planar segments and the markings perpendicular to the advancing crack front.

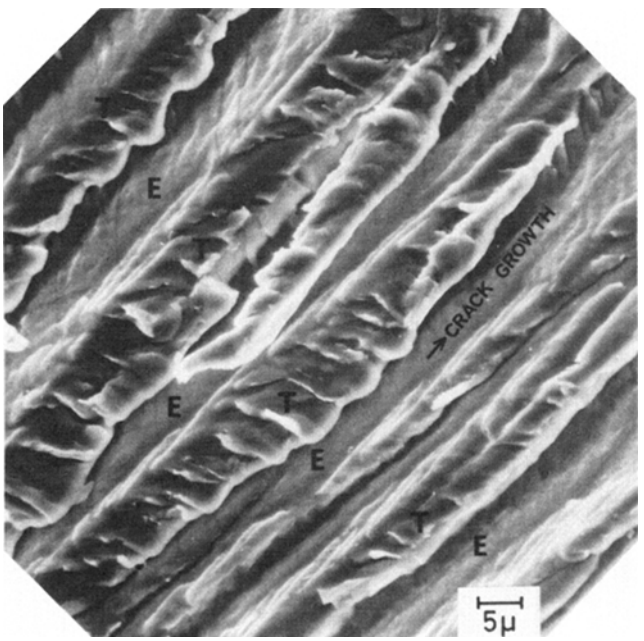

Fig. 11—Blowup of hydrogen region B in Fig. 9. Note that the crack surface appears composed of two distinct regions, E and T.

as can mechanically induced low temperature cleavage cracks, the brittle appearance of HIC can be termed as "suppressed cleavage."

C. Crack Path Transition

We have experimentally demonstrated that, comparing pure iron to iron-3 pct silicon, the HIC plane changes from the operating slip plane to the operating cleavage plane. This transition behavior has been shown to be a smooth function of silicon content. To demonstrate this, two alloys with intermediate silicon contents were used; iron-0.7 pct silicon and iron-1.4 pct silicon. Because of the presence of γ-loop on the iron-rich side of the iron-silicon binary phase dia-

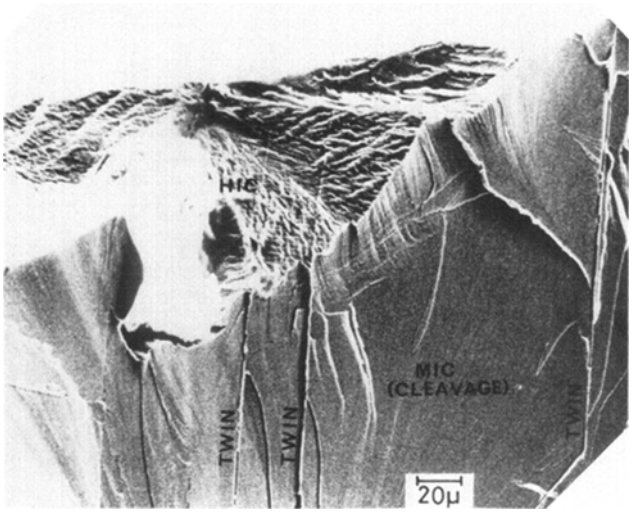

Fig. 12—Direct comparison of the hydrogen induced crack surface with the mechanically induced low temperature cleavage crack surface in Ferrovac-E iron.

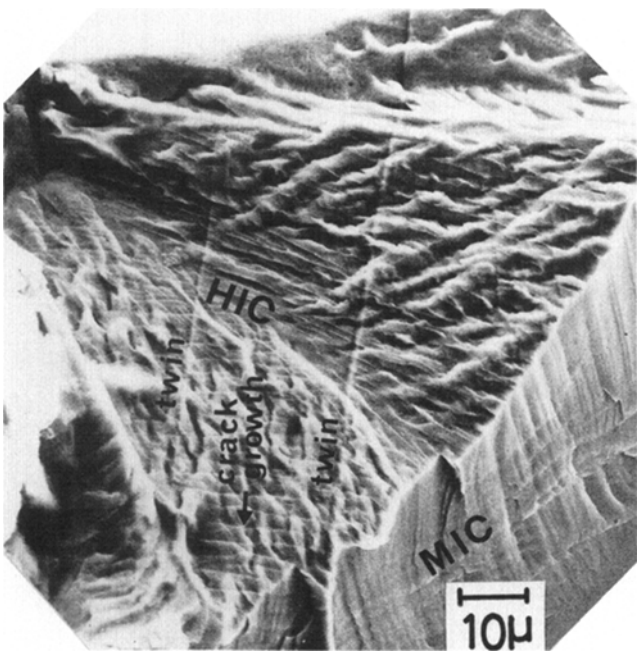

Fig. 13—Blowup of hydrogen region in Fig. 12. Similar features of the HIC surface to those in Fig. 10 show up as planar segments and the markings perpendicular to the advancing crack front.

gram, Fig. 1, the annealing temperature was limited to below the $\alpha - (\alpha + \gamma)$ boundary temperature. The resultant ferrite grain size obtained was about 200 μm, unfortunately not large enough for any surface trace analysis of hydrogen cracks to be employed. Examples of the shape and morphology of HIC in iron-0.7 pct silicon and iron-1.4 pct silicon alloys are illustrated in Fig. 15(*a*) and (*b*). In both alloys the cracks are expanded or "yawned" and indeed are more similar in appearance to HIC observed in pure iron than to those in iron-3 pct silicon, where the transgranular cracks are straight and sharp, Fig. 7. Such observations would appear to suggest that in iron-silicon alloys with 0.7 and 1.4 pct silicon content, the cracks are similar to those in purified iron and thus should

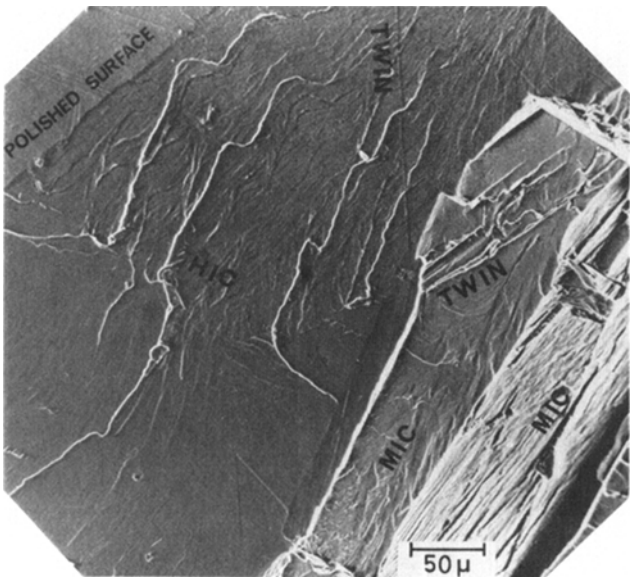

Fig. 14—Hydrogen induced cracking in an iron-3 pct silicon. Exposure of the hydrogen crack reveals the similarity of low temperature cleavage and hydrogen induced cleavage. Note the brittle nature of the crack.

lie on operating slip planes. However, detailed two dimensional fractographic studies, described below, on these two alloys show that this hypothesis is oversimplified.

Figure 16 shows the hydrogen induced transgranular crack face in iron-1.4 pct silicon, together with the mechanically induced cleavage crack surfaces and the polished surface of the specimen. In the hydrogen region, small steps are seen running parallel to each other quite similar in appearance to cleavage steps. Unlike the hydrogen region in pure iron, no evidence either for planar segments or for the markings perpendicular to the advancing crack front can be found. Such results imply that the HIC surface observed in iron-1.4 pct silicon is similar to that for iron-3 pct silicon and is essentially cleavage in nature.

On the other hand, different behavior is observed in iron-0.7 pct silicon, as shown in Fig. 17. Within the HIC surface, two distinct regions, designated A and B, are observed. Figure 18 is a higher magnification photograph of region A, and it clearly reveals the features of slip plane cracking previously observed in pure iron, the planar segments and striation patterns are perpendicular to the direction of crack propagation. In region B, however no such features can be observed; instead only small steps indicative of cleavage are present. Thus, in iron-0.7 pct silicon, the HIC surface is found to be a mixture of slip plane cracking and cleavage plane cracking, with the mix on a fairly fine scale, as seen in Fig. 17. This shows that there's a transition from slip plane to cleavage plane cracking near a silicon content of 0.7 pct.

D. *Effect of Silicon Content on* Mechanical Properties

To ascertain if this transition is accompanied by a change in mechanical properties, the tensile strength as a function of silicon content was measured, Fig. 19. The strength increases monotonically with no ap-

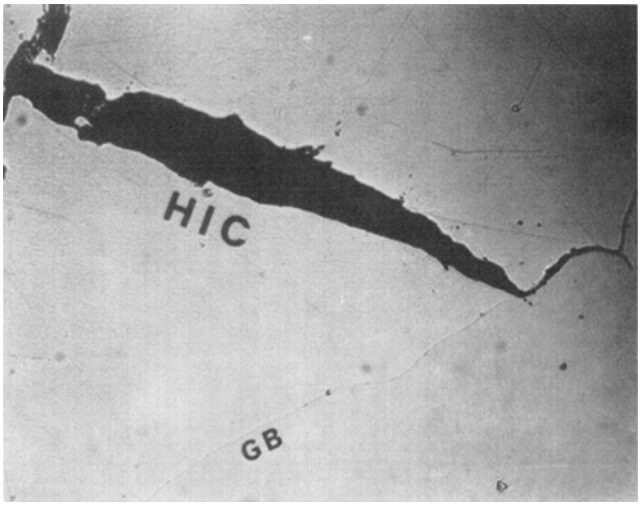

Fig. 15—The one-surface appearance of hydrogen induced cracks in Fe-0.7 pct Si (*a*) and Fe-1.4 pct Si (*b*) alloys. Note the expanded or "yawned" shape of the crack.

parent discontinuities at the transition solute content. Unfortunately lack of material prevented us from measuring tensile properties on hydrogen containing alloys.

DISCUSSION AND CONCLUSIONS

The key experimental results can be summarized as follows:

i) Even without the application of an external stress, hydrogen induced transgranular cracks can be produced which in pure iron lie on operating slip planes, while in iron-3 pct silicon, they lie on operating cleavage planes.

ii) The transition from slip plane cracking to cleavage plane cracking occurs around a silicon content of 0.7 pct.

iii) In accordance with the differences in crack plane observed in these alloys, the crack surface mor-

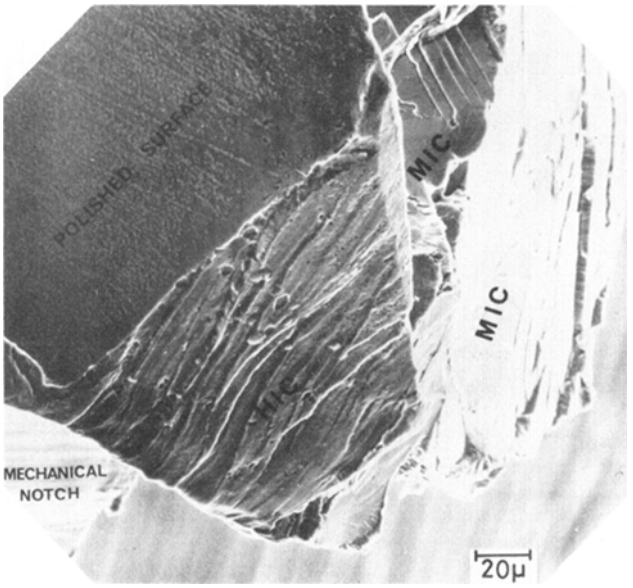

Fig. 16—Direct comparison of the hydrogen induced crack surface with the mechanically induced low temperature cleavage crack surface in iron-1.4 pct silicon. Note, in the HIC face, the absence of the evidence either for the planar segments or for the markings perpendicular to the advancing crack front.

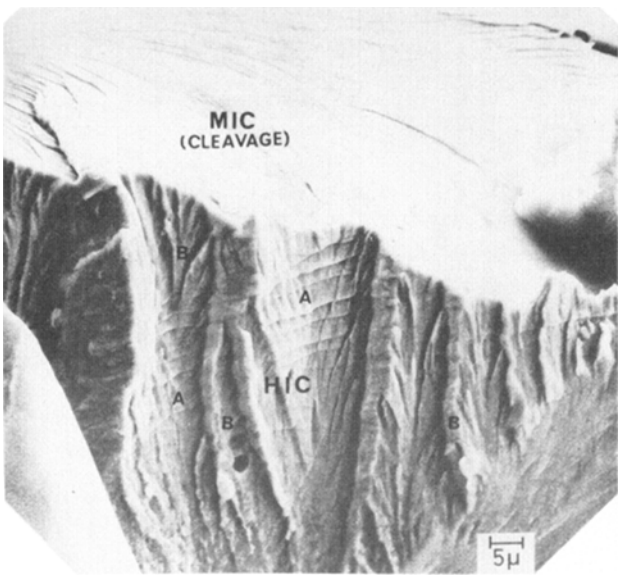

Fig. 17—Direct comparison of the HIC surface with the MIC surface in iron-0.7 pct silicon. Note that the HIC surface is composed of the two regions A and B, indicative of slip plane cracking and cleavage plane cracking, respectively.

phology is also drastically different. The HIC surface of pure iron is characterized by the presence of small planar segments and markings perpendicular to the direction of crack propagation. On the other hand, the HIC surface in iron-3 pct silicon is characterized by the presence of small and periodic steps indicative of cleavage. At intermediate silicon contents, mixed behavior is observed.

Of major interest is why the crack plane can vary in iron-base alloys. The most straightforward explanation, that it results from a strengthening of the iron lattice, (see the behavior of silicon, Fig. 19) does not appear to be generally correct. It has been experi-

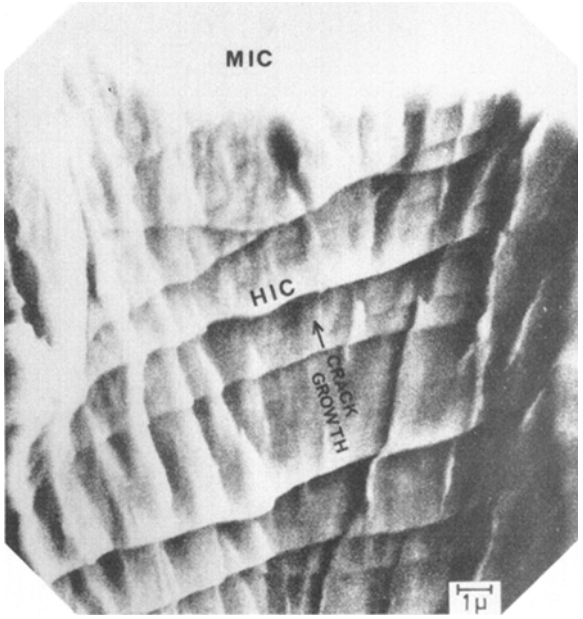

Fig. 18—Blowup of region A in Fig. 17. Note the typical appearance of the slip plane cracking.

mentally demonstrated elsewhere[2,15,16] that both 0.17 pct C-1.3 pct Mn steel with a ferrite-pearlite microstructure and 0.22 pct C-0.8 pct Mn-1.0 pct Ni-0.7 pct Cr-0.5 pct Mo steel with a tempered martensite microstructure show slip plane cracking under hydrogen-charged and externally stressed condition. The former steel has a tensile strength of 471 MPa similar to that of iron-3 pct silicon used in the present study, while the latter steel has a much higher strength of 794 MPa. Thus the strengthening effect of silicon is not a direct contributor to the crack plane transition.

A more important effect of adding silicon to pure iron is that it substantially raises the Charpy V-notch toughness transition temperature by more than 100°C, as reported in Fe-3 pct Si by Leslie.[17,18] This effect of adding silicon has been attributed to either a lowering of the cohesive energy of iron or to the restriction of cross slip promoting localized stress concentrations.[17,19] Whatever the exact mechanism might be, the matrix of iron-3 pct silicon is much more brittle than that of pure iron. Gell[20] has in fact shown that a ⟨100⟩ iron-silicon single crystal is normally brittle at room temperature, although this may not be true for other orientations. The observed difference in behavior may then be a direct function of the intrinsic toughness of the iron-alloy matrix. In low toughness alloys dislocations are generated and multiplied by local internal stresses resulting from gas recombination; dislocation interactions could then lead to the creation of small crack nucleii on {100} planes[21] particularly since cross slip is suppressed in this alloy.[4,20] Once these nuclei are formed, they can extend significant distances without blunting, aided by the internal pressure of hydrogen gas which precipitate in the crack nuclei. The cracks stop when the internal gas pressure is insufficient to provide the necessary driving force. The crack length should then be a function of hydrogen fugacity, as has been observed.[3,20] This argument suggests that in low toughness alloys hydrogen's main role can be as a local stress raiser, as suggested by many investigators.[22,24] Such an observation does not rule out as yet a more direct effect of hydrogen, say on cohesive energy.

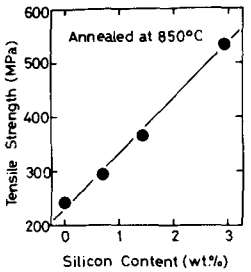

Fig. 19—Effect of silicon content on tensile strength of iron-based alloys.

In contrast, the situation in purified iron is considerably different. At room temperature, this is a highly plastic material,[6,8] and it is difficult to explain how planar microcracks can be formed solely due to stress assistance. In this case hydrogen must have a much more direct effect. Two possibilities, discussed elsewhere,[25,26] are that hydrogen preferentially reduces the cohesive energy between iron atoms perpendicular to a potential slip plane, or that it affects the relative ease of plasticity, perhaps by restricting cross slip. The fractographic studies tend to support the importance of the latter, while not ruling out a contribution from the former.

The fracture surface in iron is ratcheted in nature due to crack segmenting along slip planes which intersect the main crack face. This should require a localization of fine slip bands along such planes. Such strain localization would be aided by a reduced ease of cross slip. One way this can occur is by a reduced stacking fault energy; there is some limited evidence that this may occur for example in iron alloyed with titanium.[27] The actual slip plane separation could result from intense shear or a reduction in cohesive energy. The observed ratcheting supports the occurrence of a considerable shear offset and thus the former possibility.

The hydrogen-induced fracture surface in iron also exhibits micron-spaced markings perpendicular to the advance of the crack front, (Figs. 10, 11, 13, and 18). Although possibly slip traces, this is unlikely since traces due to other slip planes which intersect the fracture surface should also be seen. More likely, these are direct evidence for the discontinuous nature of crack advance, suggested from the results of many investigators. Finally, the cracks cease to grow when the plastic blunting from the internal stress due to precipitation of molecular hydrogen within the crack is so severe that the resulting deformation is too homogeneous to promote strain localization.

In summary, this detailed crystallographic and fractographic study has clarified how HIC are formed and grow. At least in ferritic materials, the crack plane and mode of crack advance is a function of the intrinsic toughness of the ferrite lattice. In low toughness materials, like iron-3 pct silicon, the cleavage nature of the HIC supports the suggestion,[4,14] that in this material hydrogen's major and perhaps only influence is as a local stress raiser resulting from the formation of internal molecular hydrogen. In purified iron the observations of slip plane cracking and a segmented crack surface are incompatible with this explanation. Instead it is more likely that hydrogen charging promotes highly localized slip bands on {110} or {112}; additional hydrogen charging produces high pressure within the above slip planes due to the pre-

cipitation of molecular hydrogen, facilitating the formation of cracks along slip planes.[19] From the results of the present study and those by Bernstein[8,9] and Terasaki *et al*,[2,15,16] it seems clear that slip plane cracking is a more general feature of hydrogen-induced cracking in ferrous alloys, and the iron-3 pct silicon behavior is a special case where cleavage cracking is favored.

ACKNOWLEDGMENTS

This work was supported by the Office of Naval Research under contract N00014-75-C-0265, and by Sumitomo Metal Industries, who generously provided support for F. Nakasato during his stay at Carnegie-Mellon University. The authors would like to thank Dr. J. R. Low Jr. for helpful discussions.

Note added in proof

Koch *et al*[28] have recently shown hydrogen-induced fracture surfaces in a mainly α-titanium alloy similar to those in purified iron reported here. Evidence for discontinuous cracking was also found.

REFERENCES

1. C. D. Beachem: *Met. Trans.*, 1972, vol. 3, p. 437.
2. F. Terasaki and F. Nakasato: *Proceedings of Conf. on Mechanism of Delayed Fracture Caused by Hydrogen*, p. 165, Tokyo, Japan, 1975.
3. A. S. Tetelman and W. D. Robertson: *Trans. TMS-AIME*, 1962, vol. 224, p. 775.
4. A. S. Tetelman and W. D. Robertson: *Acta Met.*, 1963, vol. 11, p. 415.
5. M. Gell and W. D. Robertson: *Acta Met.*, 1966, vol. 14, p. 481.
6. N. P. Allen, B. E. Hopkins, and J. E. McLennan: *Proc. Roy. Soc. (London)*, 1956, A234, p. 221.
7. E. Schmid and W. Boas: *Kristallplastizität*, p. 199, Springer, Berlin, 1935.
8. I. M. Bernstein: *Met. Trans.*, 1970, vol. 1, p. 3143.
9. I. M. Bernstein: *Mater. Sci. Eng.*, 1970, vol. 6, p. 1.
10. K. Kitajima: *Proceedings of Conf. on Mechanism of Delayed Fracture Caused by Hydrogen*, p. 35, Tokyo, Japan, 1975.
11. Y. Kikuta, T. Araki, and T. Kuroda: Osaka University, Osaka, Japan, unpublished research, 1974.
12. C. Ouchi and I. M. Bernstein: Carnegie-Mellon University, Pa., unpublished research, 1974.
13. F. Nakasato and I. M. Bernstein: Abstract Bulletin, TMS-AIME Fall Meeting, p. 2, Niagara Falls, New York, 1976.
14. M. Gell, J. P. Briant, and W. D. Robertson: *Trans. TMS-AIME*, 1967, vol. 239, p. 813.
15. F. Terasaki, F. Nakasato, and S. Okamoto: *Tetsu-To-Hagane*, 1973, vol. 59, p. S574.
16. F. Terasaki and S. Okamoto: *Tetsu-To-Hagane*, 1974, vol. 60, p. S576.
17. W. C. Leslie, R. J. Sober, S. G. Babcock, and S. J. Green: *Trans. ASM*, 1969, vol. 62, p. 690.
18. W. C. Leslie: *Met. Trans.*, 1972, vol. 3, p. 5.
19. C. S. Barrett: *Structure of Metals*, McGraw-Hill, New York, 1943, p. 292.
20. M. Gell: Ph.D. Thesis, Yale University, 1965.
21. A. H. Cottrell: *Trans. TMS-AIME*, 1958, vol. 212, p. 192.
22. C. Zapffe and C. Sims: *Trans. AIME*, 1941, vol. 145, p. 225.
23. C. Zapffe: *Trans. ASM*, 1947, vol. 39, p. 190.
24. A. S. Tetelman: *Fracture of Solids*, p. 671, Gordon and Breach, 1963.
25. I. M. Bernstein, R. Garber, and G. M. Pressouyre: *Effect of Hydrogen on Behavior of Materials*, A. W. Thompson and I. M. Bernstein, eds., p. 37, TMS-AIME, 1976.
26. I. M. Bernstein and A. W. Thompson: *Mechanisms of Environment Sensitive Cracking of Materials*, P. R. Swann and F. P. Ford, eds., p. 412, The Metals Society, 1978.
27. G. M. Pressouyre: Ph.D. Thesis, Carnegie-Mellon University, 1977, (also ONR report NR 036-099-7).
28. G. H. Koch, A. J. Bursle, and E. N. Pugh: *Met. Trans. A*, 1978, vol. 9A, p. 129.